ChemComm

COMMUNICATION

View Article Online
View Journal

Cite this: DOI: 10.1039/d6cc00303f

Received 15th January 2026,
Accepted 13th May 2026

DOI: 10.1039/d6cc00303f

rsc.li/chemcomm

Rapid discovery of yttrium-MOFs *via* combined high-throughput synthesis, automated PXRD, optical calorimetry screening and three-dimensional electron diffraction

Lasse Wegner,[a] Zheting Chu,[c] Tobias A. Engesser,[a] Xiaodong Zou*[c] and Norbert Stock*[abc]

An optimized workflow for the discovery of new porous materials was developed, combining high-throughput (HT) synthesis with automated powder X-ray diffraction (PXRD), high-throughput CO_2 sorption analysis and three-dimensional electron diffraction (3D ED). This led to the discovery of CAU-73, a new yttrium-based microporous metal–organic framework.

The use of high-throughput (HT) synthesis methods is an established way to screen numerous synthesis parameters and discover new compounds.[1,2] For microcrystalline materials, like metal–organic frameworks (MOFs), powder X-ray diffraction (PXRD) is typically the first technique used to identify reaction products. It offers insights into sample crystallinity and potential unit cell parameters,[3] requires only small sample quantities, and can even be fully automated.[1,4] MOFs have attracted considerable interest for gas adsorption due to their large pores. To find promising candidates among crystalline MOF products, reliable sorption analysis methods are needed.[5] Established methods such as volumetric and gravimetric sorption analysis typically require hours to days to obtain a single sorption isotherm, and commercial instruments can handle only a limited number of samples simultaneously.[6,7] In recent years, some methods like zero length columns,[8] head space gas chromatography[9] or inverse pulse gas chromatography[10] have been proposed for HT sorption evaluation, but they all require large sample amounts or are difficult to fully automate. Optical calorimetry offers an alternative, enabling measurement times of only a few minutes for multiple samples by measuring the heat released during adsorption, which is detected using an infrared sensor.[7] In addition it allows to carry out cyclic measurements to confirm stability and reproducibility.[11] The optical calorimetry approach under the name INFRAsorp has proven effective for high-throughput discovery of porous materials[12,13] and for rapid sorption screening of known materials using strongly binding adsorptives such as *n*-butane,[7] H_2S,[14] NH_3,[15] CO,[16] CO_2,[17] and H_2O.[11]

A common strategy for obtaining MOFs with targeted sorption properties is to use linkers that incorporate active sorption sites.[18–20] Heterocycle linkers, that incorporate functional groups in their ring structure, provide active sorption sites as well as a larger available pore space compared to linker molecules with external functional groups.[21–23] Especially heteroaromatic dicarboxylic acids with oxygen, sulphur and nitrogen have been used to synthesize MOFs with outstanding sorption performances, like MOF-303,[24] CAU-23[25] or MIL-160.[21] Compared to their carbon-based analogues, heteroaromatic linker molecules have been less intensively studied, especially the more complex ones like bicyclic aromatic dicarboxylates. A search of the MOF subset of the CSD (Cambridge Structural Database, as of 23.09.2025) yields 1518 deposited structures containing naphthalene dicarboxylate, but only 34 incorporating a quinoline core and just 2 using indole dicarboxylates (Fig. S1), highlighting the substantial potential for discovering new MOFs based on bicyclic N-heteroaromatic linkers. Because electrons interact much more strongly with matter than X-rays, electron diffraction enables structure determination from nano- to micrometre- sized crystals that are inaccessible to single-crystal X-ray diffraction.[26] Three-dimensional electron diffraction (3D ED) can also resolve individual crystal structures within complex or multiphase samples, where conventional PXRD often has difficulties due to peak overlap and insufficient structural information. 3D ED allows full structure solution including the framework and structural details like guests in the pores of MOFs.[27–33] By combining high-throughput PXRD and sorption analysis to rapidly screen crystallinity and gas uptake, the most promising MOF can be efficiently identified for subsequent structure–property investigations using techniques such as 3D ED to determine their crystal structures (Fig. 1).[34,35] Here, we integrate the MULTIport set-up, a HT

[a] *Institute for Inorganic Chemistry, Kiel University, Max-Eyth Straße 2, 24116, Kiel, Germany. E-mail: stock@ac.uni-kiel.de*
[b] *Kiel Nano, Surface and Interface Science KiNSIS, Kiel University, Christian-Albrechts-Platz 4, 24118, Kiel, Germany*
[c] *Department of Chemistry, Stockholm University, Svante Arrhenius väg 16 C, 106 91, Stockholm, Sweden. E-mail: xiaodong.zou@su.se*

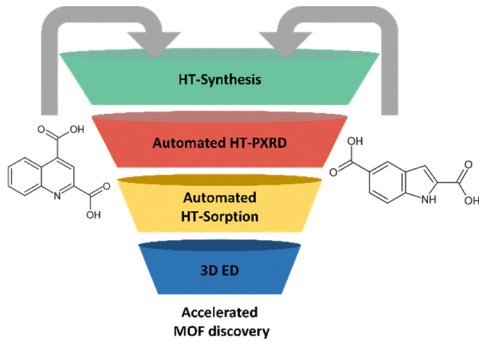

Fig. 1 Schematic overview of the optimized workflow for porous-material discovery proposed in this work.

optical calorimetry sorption device for up to twelve samples, into an HT workflow. Two N-heteroaromatic linkers were used in HT synthesis and a new microporous MOF was identified by HT PXRD and HT CO_2 sorption analysis. Structural elucidation, typically the bottleneck in MOF discovery, was achieved by 3D ED, yielding the crystal structure of a new Y-MOF: **CAU-73-2.5H$_2$O** with the composition $[Y_2(IDC)_3(H_2O)_2]\cdot 0.5\ H_2O$.

The two linker molecules 2,5-indole dicarboxylic acid (H_2IDC) and 2,4-quinoline dicarboxylic acid (H_2QDC) were employed in a metal screening experiment and 17 crystalline compounds were identified by automated HT PXRD measurements (Table S2 and Fig. S3). Based on the PXRD data, twelve samples were selected for the HT CO_2 sorption screening using the MULTIport device (Fig. 2 left). For each sample ten consecutive CO_2 ad- and desorption cycles were measured while the temperature of the sample surface was monitored. The temperature increase during CO_2 exposure is proportional to the enthalpy of adsorption and the adsorption capacity.[12] Thus, materials that show a strong temperature increase after being exposed to CO_2 are likely porous. Nevertheless, optical calorimetry is a qualitative method and a temperature increase can also be caused by strong surface interactions. The different crystalline compounds show varying responses to CO_2 gas. Some products exhibit a relatively stable signal, like Ni + H_2QDC and Bi + H_2IDC while the Y compound obtained with H_2IDC as the linker shows a temperature increase with each CO_2 sorption cycle and the highest temperature increase overall (Fig. 2 right). This indicates replacement of guest molecules, likely water, which was used as the solvent, by CO_2 molecules. To prove this hypothesis, volumetric water and CO_2 sorption experiments were conducted at 298 K (Fig. 3). The water sorption isotherm shows a steep water uptake in the low-pressure region equal to 3 mmol g^{-1} followed by a slow continuous water adsorption at higher relative pressures up to the maximum uptake of 6.6 mmol g^{-1}. In the desorption branch a hysteresis is visible down to a relative pressure of 0.3 which could be caused by framework flexibility or by capillary condensation of water being adsorbed between the heavily agglomerated crystallites (Fig. S14). For CO_2, an uptake of 0.9 mmol/g at 298 K and 1 bar is observed. The stability of the material towards the activation and measurement procedures was confirmed *via* PXRD measurements (Fig. S6). To further prove, that the sample Y-IDC had the highest porosity of the synthesized samples, CO_2 sorption isotherms of the five products with the highest temperature increase in the optical calorimetry screening were collected and compared, showing that only Y-IDC exhibits significant porosity towards CO_2 (Fig. S4). 3D ED was used for structure determination of the most promising candidate (Y + IDC) from optical calorimetry screening, which was given the name **CAU-73**. The crystal structures of **CAU-73** with three different degrees of hydration were obtained from 3D ED data under high vacuum (Table S3): a) at 100 K (**CAU-73-2.5H$_2$O**), b) at 298 K (**CAU-73-H$_2$O**) and c) at 523 K (**CAU-73**). The **CAU-73** compounds crystallize in the triclinic space group $P\bar{1}$ and adopt the fsy-topology known from lanthanide coordination polymers with the general sum formula $[Ln_2L_3]$.[36–38] There are two crystallographically independent $[YO_6(H_2O)_n]$ (n = 0–1) polyhedra, which are connected *via* the carboxylate groups of six IDC linkers into a hybrid chain along the crystallographic *a*-axis. Each chain is connected to four other chains through six IDC linkers to form a 3D framework with two potential pore channels (Fig. S8–S10).

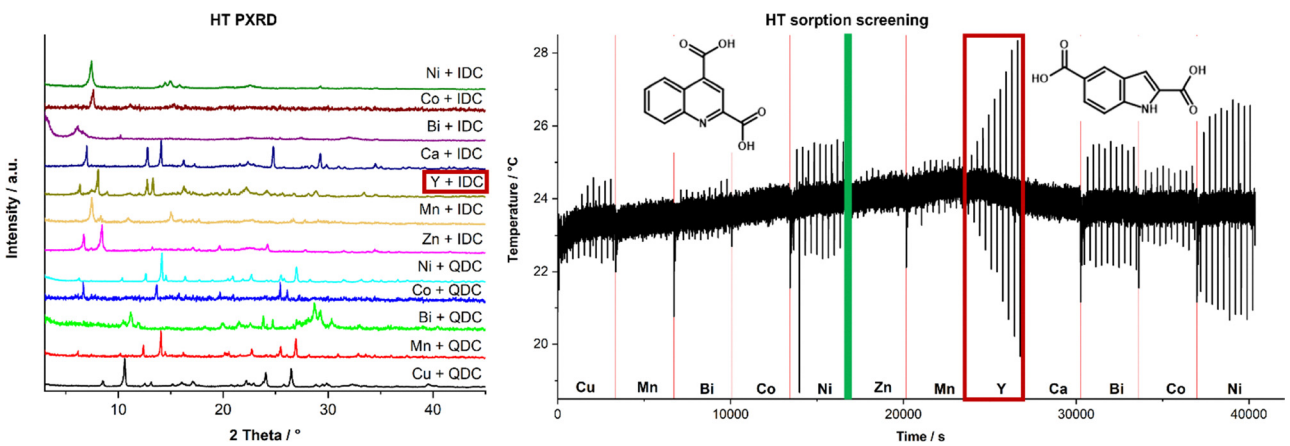

Fig. 2 Left: PXRD patterns of the 12 samples that were chosen for the CO_2 sorption screening with the MULTIPORT. Right: Results of the HT-porosity screening with CO_2 at ambient temperature. For each sample, ten ad- and desorption cycles were measured consecutively. The data for the reaction product Y + IDC has been marked with a red box.

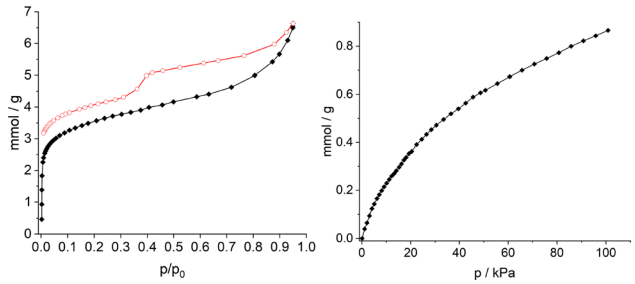

Fig. 3 Sorption analysis of **CAU-73** after activation of the material at 200 °C under reduced pressure Bottom: Water sorption isotherms of **CAU-73** recorded at 298 K. The adsorption branch is shown as black diamonds and the desorption with red circles. Top: CO_2 sorption isotherm recorded at 298 K.

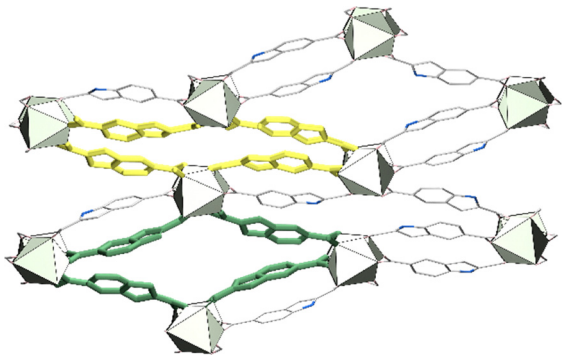

Fig. 4 Framework of **CAU-73** seen along [100] with the two different pores highlighted in green and yellow. Carbon atoms are shown in grey, nitrogen in blue, yttrium in green and carboxylic oxygen atoms in pink.

At low temperature (100 K), one water molecule is coordinated to each of the two yttrium ions. Furthermore, one physisorbed water molecule is found in one of the channels, while the other one is closed due to hydrogen bonding interactions (Fig. S8). At room temperature (298 K), the physisorbed water and the coordinated water molecule of one yttrium ion are removed (Fig. S9). No water molecule is found from the data collected at 525 K (Fig. S10). Since the structures of the three compounds are very similar apart from the water content, the framework of the fully dehydrated phase is depicted representatively in Fig. 4, showing the large pore channels in green and the small ones in yellow. Details of the structure determination and structure description of the **CAU-73** structures are reported in the SI (Sections S6 and S7). PXRD confirms that the synthesis product corresponds to the fully hydrated **CAU-73·2.5H$_2$O** (Fig. S7). Our results show, that the physisorbed water molecules and the coordinating water molecules that point into the open pore can be removed stepwise, *i.e.* under reduced pressure and *via* increased temperatures, which trigger the phase changes of the compounds. To gain further insight into the water desorption process and the accompanied phase changes in **CAU-73**, we conducted variable temperature powder X-ray diffraction (VT-PXRD) and diffuse reflectance infrared Fourier transform spectroscopy (DRIFTS) experiments in the temperature range from 20 °C to 400 °C (Fig. 5 left and centre). In the VT-PXRD data, two phase changes are visible, the first occurs at *ca.* 125 °C and the second one at 200–225 °C. Above 350 °C the material begins to lose its crystallinity which is in line with the decomposition seen in the TG data that sets in at around 365 °C. The phase transition temperatures are summarized in Table 1. The DRIFTS data shows the spectral range typical for OH and NH vibrations. The spectrum recorded at 20 °C shows six individual

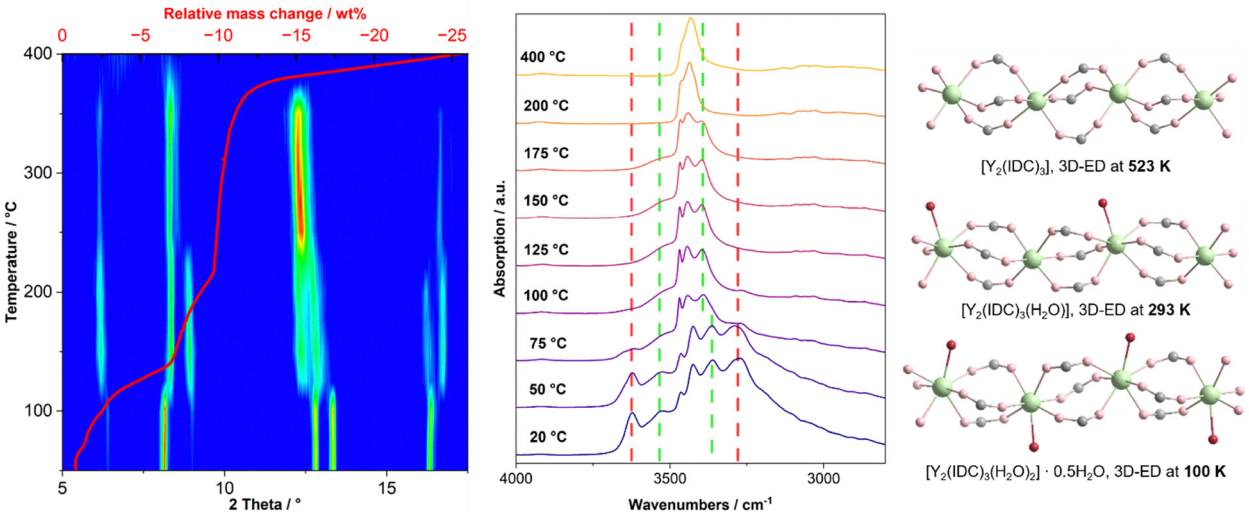

Fig. 5 Left: Variable temperature XRD measurements of CAU-73 overlayed with the TG curve of **CAU-73** showing two phase changes at 125 °C and 200–225 °C. Centre: Diffuse Reflectance Infrared Fourier Transform (DRIFT) spectra of **CAU-73** from 200 °C to 400 °C in the range from 1800 cm^{-1} to 4000 cm^{-1}. The dashed red lines at 3279 cm^{-1} and 3535 cm^{-1} are marking bands of OH-vibrations that are disappearing at 125 °C while the dashed green lines at 3363 cm^{-1} and 3535 cm^{-1} mark the OH-bands that are disappearing at 200 °C. Unmarked bands at 3427 cm^{-1} and 3466 cm^{-1} that remain until 400 °C belong to the NH vibration of the linker molecule. Right: Comparison of the chain like hybrid IBU running along [100] of **CAU-73** in the fully hydrated, partially dehydrated, and the fully activated compound. Yttrium atoms are depicted in green, oxygen in pink, carbon in grey and water molecules in red.

Table 1 List of phase transition temperatures of **CAU-73** obtained from VT-PXRD data

	Temperature VTXRD/°C
Phase transition 1	125
Phase transition 2	200–225
Decomposition	>350

bands in the range from 3000 cm^{-1} to 4000 cm^{-1}. By comparing the spectrum with the one of the pristine linker molecule (Fig. S11), the bands at 3427 cm^{-1} and 3466 cm^{-1} can be assigned to the NH stretching vibration of the indole group while the other four bands can be assigned to the OH stretching vibrations of the two coordinating water molecules present in the compound. The broad band from 2800 cm^{-1} to 3600 cm^{-1} can be attributed to the presence of water molecules occupying the pores of the material, which can be desorbed at relatively low temperatures of around 75 °C as seen by the decrease in intensity in this region above 50 °C. This also leads to a change in the hydrogen bonding environment of one of the coordinating water molecules, shifting the OH vibration at 3363 cm^{-1} to 3393 cm^{-1}. From 100 °C to 125 °C, the bands marked in red at 3279 cm^{-1} and 3625 cm^{-1} disappear, signalling the desorption of the first coordinating water molecule at the same temperature where the first phase change in the VT-PXRD data is visible. From 175 °C to 200 °C, the second coordinating water molecule is desorbed as seen by the disappearance of the bands marked in green at 3393 cm^{-1} and 3535 cm^{-1}, which coincides with the second phase change seen in the VT-PXRD data. The thermal desorption of the water molecules from **CAU-73** can also be seen in the TG data, where three mass losses can be identified in the solvent region up to 220 °C, before the material starts to decompose above 365 °C (Fig. 5 left).

In this study we leveraged the INFRAsorp technology to rapidly screen the reaction products of twelve different metal salts with 2,4-quinoline dicarboxylic acid and 2,5-indole dicarboxylic acid for potentially porous compounds. This resulted in the discovery of the microporous Y-MOF **CAU-73** of composition $[Y_2(IDC)_3(H_2O)_2]\cdot 0.5\ H_2O$ that is porous towards CO_2 and water at room temperature. Through a combination of 3D ED, VT-PXRD and VT-DRIFT, we were able to unravel the structural evolution of **CAU-73**, which undergoes two phase changes upon desorption of its coordinating water molecules, changing its sum formula from $[Y_2(IDC)_3(H_2O)_2]\cdot 0.5\ H_2O$ at ambient conditions to $[Y_2(IDC)_3(H_2O)]$ at 125 °C and to $[Y_2(IDC)_3]$ at 200 °C. Our proposed workflow combining high-throughput synthesis, automated PXRD, optical calorimetry screening, and 3D ED can significantly accelerate the discovery of new porous materials.

Conflicts of interest

There are no conflicts to declare.

Data availability

The data supporting this article have been included as part of the supplementary information (SI). Supplementary information: this data includes the materials and methods section, further structural and characterisation data (PXRD data, elemental and thermogravimetric analysis data, IR spectra and sorption isotherms). See DOI: https://doi.org/10.1039/d6cc00303f.

CCDC 2518146 (**CAU-73**), 2518147 (**CAU-73-H_2O**) and 2518148 (**CAU-73-2.5H_2O**) contain the supplementary crystallographic data for this paper.[39a–c]

Acknowledgements

L. W. and N. S. thank the German Science Foundation for financial support (project: STO-643/14-1). We thank Dr Andrew Kentaro Inge for assisting with the VT-PXRD measurement in Stockholm University.

References

1 I. G. Clayson, D. Hewitt, M. Hutereau, T. Pope and B. Slater, *Adv. Mater.*, 2020, **32**, e2002780.
2 H. Reinsch and N. Stock, *Microporous Mesoporous Mater.*, 2013, **171**, 156–165.
3 A. J. Howarth, A. W. Peters, N. A. Vermeulen, T. C. Wang, J. T. Hupp and O. K. Farha, *Chem. Mater.*, 2017, **29**, 26–39.
4 N. Stock, *Microporous Mesoporous Mater.*, 2010, **129**, 287–295.
5 H. Furukawa, K. E. Cordova, M. O'Keeffe and O. M. Yaghi, *Science*, 2013, **341**, 1230444.
6 A. D. Wiersum, C. Giovannangeli, D. Vincent, E. Bloch, H. Reinsch, N. Stock, J. S. Lee, J.-S. Chang and P. L. Llewellyn, *ACS Comb. Sci.*, 2013, **15**, 111–119.
7 P. Wollmann, M. Leistner, W. Grählert, O. Throl, F. Dreisbach and S. Kaskel, *Microporous Mesoporous Mater.*, 2012, **149**, 86–94.
8 X. Hu, S. Brandani, A. I. Benin and R. R. Willis, *Ind. Eng. Chem. Res.*, 2015, **54**, 6772–6780.
9 J. M. Young, S. H. McCalmont, S. Fourmentin, P. Manesiotis, J. D. Holbrey and L. Moura, *ACS Sustainable Chem. Eng.*, 2023, **11**, 17787–17796.
10 K. Yusuf, O. Shekhah, Z. ALOthman and M. Eddaoudi, *Appl. Sci.*, 2021, **11**, 10243.
11 M. Wöllner, N. Klein and S. Kaskel, *Microporous Mesoporous Mater.*, 2019, **278**, 206–211.
12 P. Wollmann, M. Leistner, U. Stoeck, R. Grünker, K. Gedrich, N. Klein, O. Throl, W. Grählert, I. Senkovska, F. Dreisbach and S. Kaskel, *Chem. Commun.*, 2011, **47**, 5151–5153.
13 M. Leistner, W. Grählert and S. Kaskel, *Chem. Ing. Tech.*, 2013, **85**, 747–752.
14 F. Sandra, N. Klein, M. Leistner, M. R. Lohe, M. Benusch, M. Woellner, J. Grothe and S. Kaskel, *Ind. Eng. Chem. Res.*, 2015, **54**, 6677–6682.
15 A. Werner, M. Wöllner, P. Bludovsky, M. Leistner, C. Selzer and S. Kaskel, *Microporous Mesoporous Mater.*, 2018, **268**, 46–49.
16 K. Wegner, M. Wöllner, R. Zippel, M. Medicus, E. Schade, J. Grothe and S. Kaskel, *Ind. Eng. Chem. Res.*, 2019, **58**, 19839–19846.
17 S. Mazzanti, S. Cao, K. ten Brummelhuis, A. Völkel, J. Khamrai, D. I. Sharapa, S. Youk, T. Heil, N. V. Tarakina, V. Strauss, I. Ghosh, B. König, M. Oschatz, M. Antonietti and A. Savateev, *Appl. Catal., B*, 2021, **285**, 119773.
18 S. Ali Akbar Razavi and A. Morsali, *Coord. Chem. Rev.*, 2019, **399**, 213023.
19 P. Á. Szilágyi, I. Weinrauch, H. Oh, M. Hirscher, J. Juan-Alcañiz, P. Serra-Crespo, M. de Respinis, B. J. Trześniewski, F. Kapteijn, H. Geerlings, J. Gascon, B. Dam, A. Grzech and R. van de Krol, *J. Phys. Chem. C*, 2014, **118**, 19572–19579.
20 Z. H. Rada, H. R. Abid, H. Sun, J. Shang, J. Li, Y. He, S. Liu and S. Wang, *Prog. Nat. Sci.: Mater. Int.*, 2018, **28**, 160–167.
21 A. Cadiau, J. S. Lee, D. Damasceno Borges, P. Fabry, T. Devic, M. T. Wharmby, C. Martineau, D. Foucher, F. Taulelle, C.-H. Jun, Y. K. Hwang, N. Stock, M. F. de Lange, F. Kapteijn, J. Gascon, G. Maurin, J.-S. Chang and C. Serre, *Adv. Mater.*, 2015, **27**, 4775–4780.
22 K. H. Cho, D. D. Borges, J. S. Lee, J. Park, S. J. Cho, D. Jo, U.-H. Lee, G. Maurin and J.-S. Chang, *ACS Sustainable Chem. Eng.*, 2022, **10**, 7010–7019.
23 Y. Hu, L. Wang, R. Nan, N. Xu, Y. Jiang, D. Wang, T. Yan, D. Liu, Y. Zhang and B. Chen, *Chem. Eng. J.*, 2023, **471**, 144851.

24 N. Hanikel, M. S. Prévot, F. Fathieh, E. A. Kapustin, H. Lyu, H. Wang, N. J. Diercks, T. G. Glover and O. M. Yaghi, *ACS Cent. Sci.*, 2019, **5**, 1699–1706.
25 D. Lenzen, J. Zhao, S.-J. Ernst, M. Wahiduzzaman, A. Ken Inge, D. Fröhlich, H. Xu, H.-J. Bart, C. Janiak, S. Henninger, G. Maurin, X. Zou and N. Stock, *Nat. Commun.*, 2019, **10**, 3025.
26 R. Henderson, *Q. Rev. Biophys.*, 1995, **28**, 171–193.
27 X. Zou, *Electron Crystallography. Electron Microscopy and Electron Diffraction*, Oxford University Press Incorporated, Oxford, 2011.
28 D. Shi, B. L. Nannenga, M. G. Iadanza and T. Gonen, *eLife*, 2013, **2**, e01345.
29 Y. Yun, W. Wan, F. Rabbani, J. Su, H. Xu, S. Hovmöller, M. Johnsson and X. Zou, *J. Appl. Cryst.*, 2014, **47**, 2048–2054.
30 M. Gemmi, M. Merlini, L. Palatinus, P. Fumagalli and M. Hanfland, *Am. Min.*, 2016, **101**, 2645–2654.
31 L. Palatinus, P. Brázda, P. Boullay, O. Perez, M. Klementová, S. Petit, V. Eigner, M. Zaarour and S. Mintova, *Science*, 2017, **355**, 166–169.
32 M. O. Cichocka, J. Ångström, B. Wang, X. Zou and S. Smeets, *J. Appl. Cryst.*, 2018, **51**, 1652–1661.
33 Z. Huang, E. S. Grape, J. Li, A. K. Inge and X. Zou, *Coord. Chem. Rev.*, 2021, **427**, 213583.
34 Z. Huang, T. Willhammar and X. Zou, *Chem. Sci.*, 2020, **12**, 1206–1219.
35 T. Yang, T. Willhammar, H. Xu, X. Zou and Z. Huang, *Nat. Protoc.*, 2022, **17**, 2389–2413.
36 S. Zhang, W. Shi, L. Li, E. Duan and P. Cheng, *Inorg. Chem.*, 2014, **53**, 10340–10346.
37 G. Liu, X. Li and X. Ren, *J. Rare Earths*, 2011, **29**, 511–515.
38 S. C. Manna, E. Zangrando, A. Bencini, C. Benelli and N. R. Chaudhuri, *Inorg. Chem.*, 2006, **45**, 9114–9122.
39 (*a*) CCDC 2518146: Experimental Crystal Structure Determination, 2026, DOI: 10.5517/ccdc.csd.cc2qjbj4; (*b*) CCDC 2518147: Experimental Crystal Structure Determination, 2026, DOI: 10.5517/ccdc.csd.cc2qjbk5; (*c*) CCDC 2518148: Experimental Crystal Structure Determination, 2026, DOI: 10.5517/ccdc.csd.cc2qjbl6.